Hindawi
International Journal of Antennas and Propagation
Volume 2021, Article ID 5567417, 15 pages
https://doi.org/10.1155/2021/5567417

Research Article

A Novel "回" Pane Structure Multiband Microstrip Antenna for 2G/3G/4G/5G/WLAN/Navigation Applications

Zhen Yu, Ziheng Lin, Xiaoying Ran, Yao Li, Bing Liang, and Xiaoyan Wang

North China Institute of Science and Technology, Langfang 101601, China

Correspondence should be addressed to Xiaoying Ran; starsky202@ncist.edu.cn

Received 10 January 2021; Revised 13 April 2021; Accepted 25 May 2021; Published 16 June 2021

Academic Editor: Rodolfo Araneo

This work proposes a novel multiband slotted planar antenna with a "回" structure, which is similar to an ancient Chinese window grille structure. The antenna is suitable for wireless applications, including the second-generation (2G), third-generation (3G), fourth-generation (4G), and fifth-generation (5G) technologies, as well as WLAN and navigation applications. The proposed antenna is based on the structural characteristics of a conventional monopole antenna, which combines the advantages of a slit structure and microstrip line structure for feeding. It adopts a circular patch with a slit structure placed in it, which is similar to the Chinese classical pane structure. This structure enables an effective reduction of the size of the antenna. The four-sided "回" gaps change the path of current flow and are coupled to each other, improving the impedance matching and radiation characteristics of the entire target frequency band. The antenna covers the frequency ranges of 1.58–1.77 GHz (12%), 2.1–2.50 GHz (17%), 3.61–4.09 GHz (12%), and 4.75–6.5 GHz (36%), permitting more than 10 wireless applications in these 4 frequency bands. This antenna uses an FR-4 dielectric material; the relative dielectric constant of the dielectric plate is 4.4, and the actual dimensions of the antenna are $85 \times 70 \times 1.6\ \text{mm}^3$. The test and simulation results are in good agreement with each other, thus confirming that the proposed design method meets the requirements of various wireless applications.

1. Introduction

With wireless applications becoming increasingly more popular, the requirements for antenna miniaturisation, multiple frequency bands, and ease of loading have grown considerably. In order to achieve multiple frequency bands, antennas are commonly designed with multiple feed points, and a U-shaped reflector is included at the bottom to expand the frequency band [1]. Antennas can also be designed for multiple iterations to improve their performance. For example, the square and circle antenna designs similar to ancient Chinese coins have been shown to exhibit good performance after a five-layer iteration [2]. Multiband and broadband characteristics of antennas can be achieved through the use of coupling and feed-matching circuits [3]. At present, many multiband antennas have been proposed [4, 5]. Additionally, different feeding methods have been utilised: although the microstrip line feeding performs well in terms of losses, the resulting frequency band is narrow [6–8]. Coplanar waveguide (CPW) designs also have some advantages and disadvantages [9, 10].

Therefore, it is necessary to eliminate the shortage of microstrip feed. Many methods have also been used to design multiband antennas, such as fractal-structure antennas, geometric shapes, Koch snowflakes, and Hilbert curves. Fractal antennas have been mainly designed following two different methods, namely, self-similarity [11, 12] and space filling [13, 14]. Self-similarity in fractal antennas permits the achievement of similar surface current distributions in different planes as well as multifrequency characteristics; space filling enables the increase of the antenna electrical length [15, 16]. Furthermore, it has been shown that the frequency band of antennas can be increased by adding branches and slits [17, 18]. In order to reduce the size of antennas, it is important to note that the size of the dielectric resonant antenna (DRA) is proportional to the parameter $\lambda/\varepsilon_r^{1/2}$. Increasing the relative dielectric constant of the antenna medium can thus effectively reduce the

antenna size [19]. In terms of improving impedance matching and radiation characteristics, a loading slot can be used to couple the same stub to the radiating element, and the stub is coupled to the local ground [20]. It is also possible to load a double T-shaped structure inside the elliptical ring structure to improve the −10 dB impedance bandwidth of the antenna without affecting the compactness of the antenna [21].

However, the frequency bands of traditional monopole antennas and dipole antennas are often narrow and cannot meet the requirements due to antenna resonance. Therefore, in order to design a miniaturised, low-profile multiband planar antenna that can be used for mobile terminals, it is necessary to combine patch slotting or fractal geometry with traditional antennas. The comparison between this article and previous studies is shown in Table 1.

This work proposes a multiband planar antenna with a circular monopole patch as the main radiator and a slotted design in the patch. Its shape is similar to that of a Chinese classical "回" pattern pane. The antenna covers multiple frequency bands: GPS (1.575–1.625 GHz), DCS (1.71–1.88 GHz), Bluetooth (2.4–2.485 GHz), WLAN (2.4–2.4835 GHz), LTE Band40 (2300–2400 MHz), ISM Band (2.420–2.4835 GHz), WiMAX (2.3 GHz), SCDMA (1.880–2.025 MHz and 2.300–2.400 MHz), LTE42/43 (3.4–3.8 GHz), WiMAX (3.3–3.8 GHz), WLAN (802.11a/n: 5.15–5.35 GHz), and 5G (5.725–5.825 GHz). As shown in Table 1, the size and performance of the antennas in this work are compared with those mentioned in the references.

2. Antenna Structure and Design Procedure

2.1. Characteristics of the Antenna Structure. The length and width of the radiator are calculated according to well-known mathematical equations:

$$f = \frac{c}{2L\sqrt{\varepsilon_r}}, \tag{1}$$

where L is the length of the antenna radiator, f is the centre frequency of the antenna during operation, c is the speed of light in free space (3×10^8 m/s), and ε_r is the dielectric constant of the dielectric plate.

The structure and parameters of the microstrip feeder planar antenna are shown in Figure 1, and the size is shown in Table 2. The antenna is connected to a 50 Ω microstrip feeder on a circular patch with slits, with a ground layer on the back, and its pattern is similar to the ancient Chinese "回" pattern pane, as shown in Figure 2. In the traditional Chinese culture, window panes were often carved in phoebe, decorated on doors, windows, and partitions, and carved with different patterns to increase the lighting surface of the room and increase the space transparency. The "回" pattern was originally derived from the thunder pattern on ancient pottery and bronze. In China, lines are flexible, and intermittent sorting implies endless life, auspiciousness, and peace. This pattern can be used to increase the length of the radiator in order to extend the electrical length and radiation efficiency of the antenna. The antenna was designed on an FR-4 substrate with a thickness of 1.6 mm, a dielectric constant of 4.4, and a loss tangent of 0.02.

As shown in Figure 3, the "回" structure was engraved inside the antenna. The principle of this structure is also derived from the traditional monopole antenna. Therefore, the length of the low-radiation patch can be calculated as

$$L_{\text{low}} \approx L_1 + L_2 + L_3 + L_4 + L_5 + L_6 + L_7 = 56\,\text{mm},$$
$$f_1 = \frac{c}{2L_a\sqrt{\varepsilon_r}} \approx 1.33\,\text{GHz}. \tag{2}$$

At high frequencies, current flows through all the gaps. And it resonates with the surrounding gaps. The current flows through about one-third of L_4. From the data given in Table 2,

$$L_{\text{high}} \approx \frac{L_6 + L_7 + L_2}{5} = 13.2\ \text{mm},$$
$$f_2 = \frac{c}{2L_b\sqrt{\varepsilon_r}} \approx 5.68\ \text{GHz}. \tag{3}$$

2.2. Simulation Results. The simulation was performed using Ansoft High-Frequency Simulation Software (HFSS) (version 18.0). Figure 4(a) illustrates a monopole antenna with a cross-slit inside a circular patch. The slit size is fixed, resulting in four resonance frequency bands, namely, 1.5, 1.9, 2.4, and 4 GHz. From Figure 4(b), it can be seen that the first-order slits are placed along the four directions of the circular patch, resulting in four frequency bands, i.e., 1.90–2.68 GHz, 3.50–4.11 GHz, 4.32–4.65 GHz, and 5.48–6.17 GHz. The isolation of the two central frequency bands is low, and the return loss performance of the high-frequency band is poor. Figure 4(c) shows a second-order slit on the basis of Figure 4(b) so that the antenna resonance frequency band tends to stabilise at 1.7, 2.4, 3.8, and 4.95 GHz. Figure 4(d) displays a change in the three parameters L_1, L_2, and W. The above four parameters were optimised and analysed in order to obtain an antenna return loss performance suitable for the applicable ranges of GPS, WLAN, 5G, and other commercial frequency bands. When the antenna was derivatized, the change of the antenna frequency band is shown in Table 3.

As shown in Figure 5, the length of L_4 is swept from 4.4 mm to 8.2 mm. Under different lengths, it is found that S11 does not change significantly in the high-frequency band. When the length of L_4 changes, the frequency band shifts from 1.2 to 1.8 GHz. After comparison, $L_4 = 5$ mm is the best frequency band. As shown in Figure 6, there is no obvious change in the low-frequency range when L_7 is at 5.2–6.8 mm. When the frequency band is 5–6.5 GHz, $L_7 = 6$ mm achieves the best performance.

As shown in Figure 7, the length of H was swept from 10 mm to 85 mm to change the size of the background plane. When $H = 10$ mm, the return loss performance in the low-frequency band is poor and cannot meet the requirements of the commercial frequency band. Gradually increase the length H of the ground plate. When $H = 55$ mm, there are multiple

Table 1: Performance comparison of the proposed antenna with the recent pioneering state of the art.

Reference	Dimension (mm^3)	Operating bands (GHz)	Substrate	Gain (dBi)	Efficiency (%)	Feeding technique
[1]	$144 \times 132 \times 2$	2G/3G/4G	Aluminum	5	47.3	Microstrip
[2]	$88.5 \times 60 \times 1.6$	1.6/2.6/3.7/5.3	FR-4	3.75	72	CPW
[4]	$40 \times 30 \times 0.81$	5G/WLAN	Taconic TLY-5	NG	NG	Microstrip
[12]	$31 \times 25 \times 1.524$	2/3/4.5/5.2	Rogers RO4350B	5.67	NG	CPW
[15]	$20 \times 21 \times 1$	8.67	FR-4	NG	NG	Microstrip
[17]	$50 \times 45 \times 1.6$	0.9/1.5/2.4/3.8/5.6/6.9	FR-4	3.45	NG	CPW
[20]	$30 \times 40 \times 1.6$	n77/n78/n79 and WLAN	FR-4	3.5	85	Microstrip
[21]	$20 \times 8.7 \times 0.4$	5/6	FR-4	2.25	80	CPW
This work	$85 \times 70 \times 1.6$	1.6/2.35/3.8/5.85	FR-4	5.9	81	Microstrip

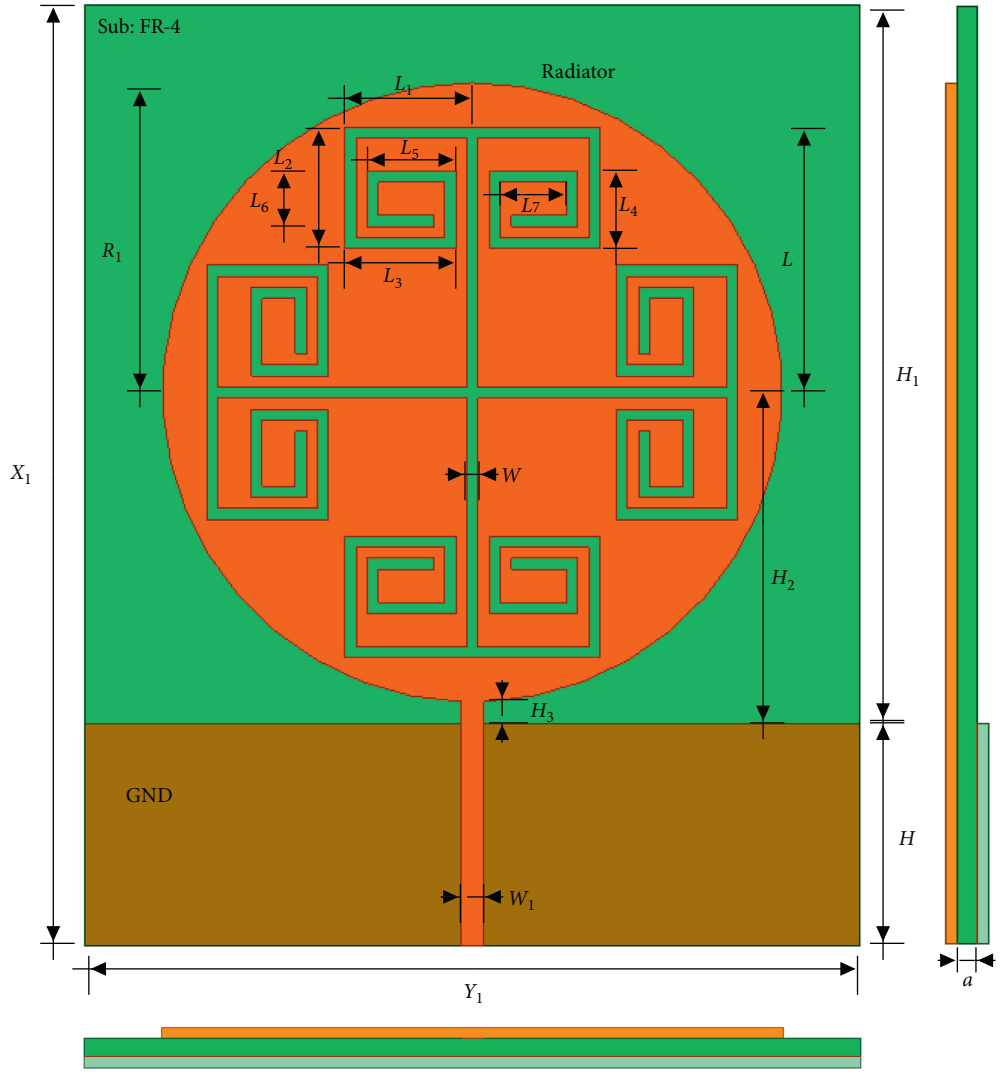

Figure 1: Layout of the proposed antenna.

Table 2: Dimensions of the proposed antenna.

Dimensions' parameters	X_1	Y_1	H	H_1	H_2	H_3	$R1$	W	$W1$	L	$L1$	$L2$	$L3$	$L4$	$L5$	$L6$	$L7$	a
Unit (mm)	85	70	20	65	30	2	28	1	2	24	11	11	10	5	8	5	6	1.6

frequency bands at low frequency, but the isolation between the frequency bands is poor, which is easy to cause mutual interference between the frequency bands. The maximum size of the grounding plate is $H = 85$ mm, and the return loss obtained is not appropriate. Therefore, the most suitable size of $H = 20$ mm is used to design the grounding plate.

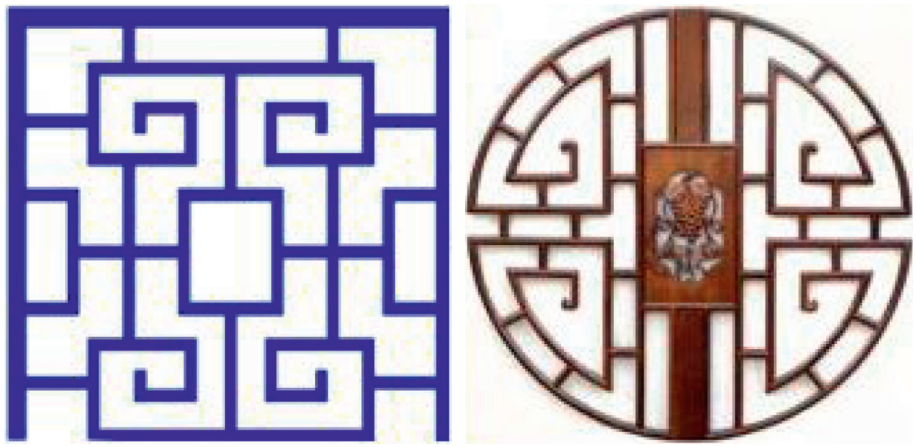

Figure 2: Photographs of the ancient Chinese "回" pane.

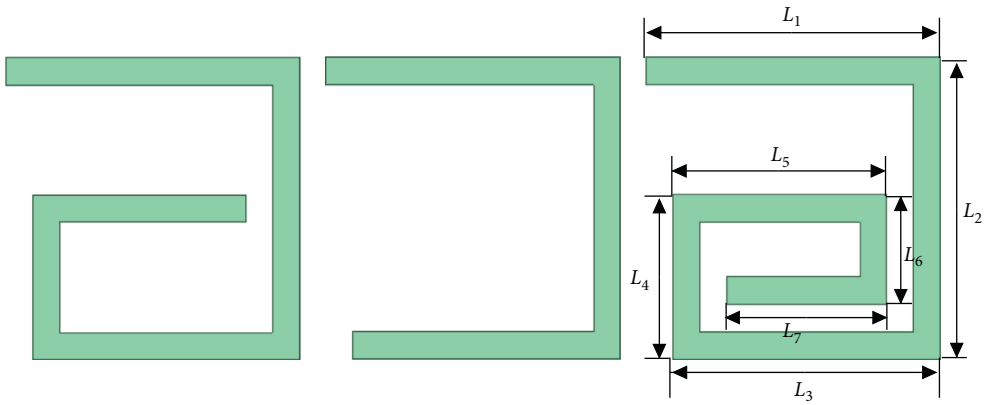

Figure 3: "回" pane structure model.

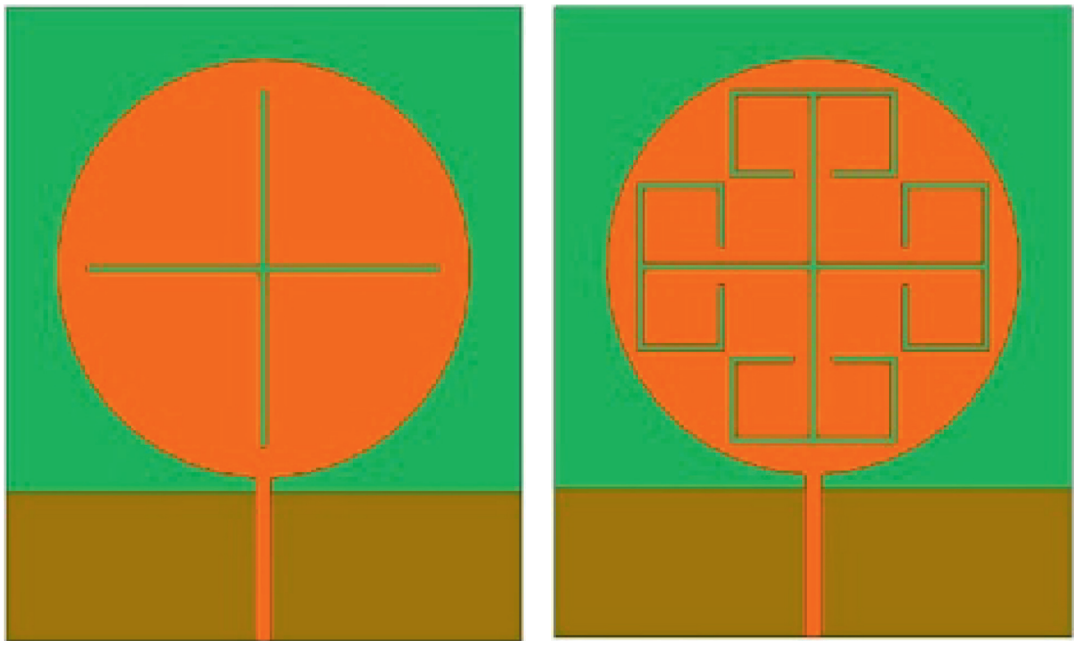

(a) (b)

Figure 4: Continued.

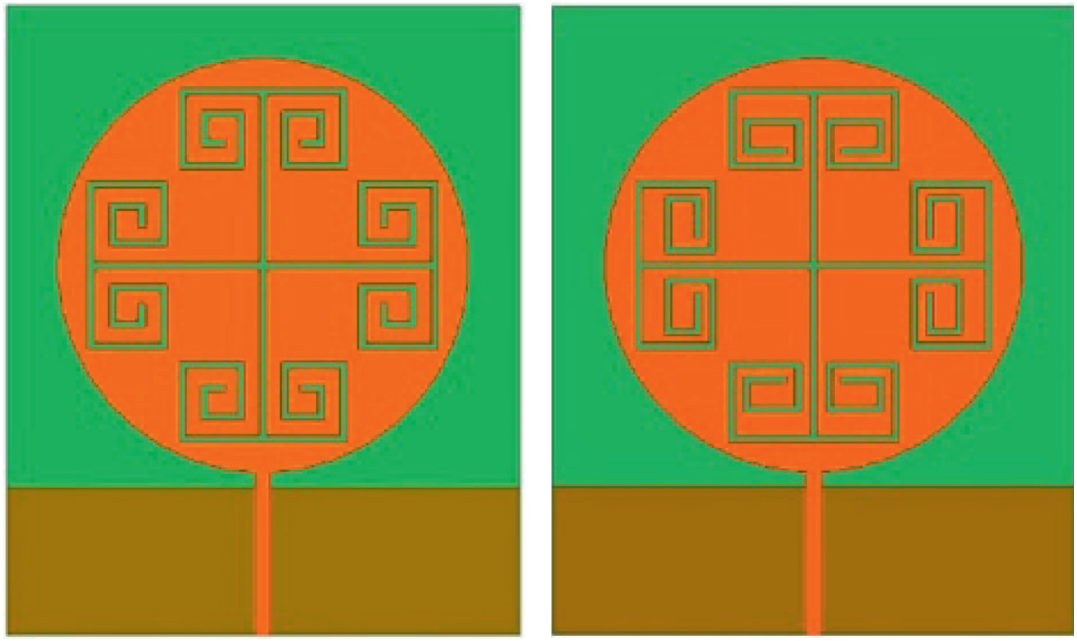

(c) (d)

Figure 4: Antenna evolution process structure diagram.

Table 3: Changes in the frequency band when antennas are derived.

Antenna no.	Bandwidth
a	1.35–1.65 GHz, 1.75–1.95 GHz, 2.05–2.85 GHz, and 3.55–6.35 GHz
b	1.90–2.68 GHz, 3.50–4.11 GHz, 4.32–4.65 GHz, and 5.48–6.17 GHz
c	1.5–1.9 GHz, 2.15–2.6 GHz, and 3.65–6.1 GHz
d	1.36–1.77 GHz, 1.96–2.50 GHz, 3.54–4.09 GHz, and 5.07–6.25 GHz

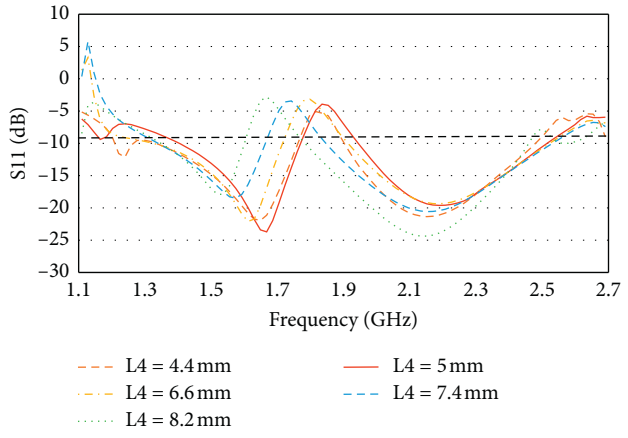

Figure 5: Variation of S11 (dB) for various L_4 lengths.

As shown in Figure 8, the proposed antenna can work in four different frequency bands: the centre frequency points are 1.6, 2.35, 3.8, and 5.85 GHz, and the corresponding return losses are −23.5, −21.5, −15.2, and −22.5 dB. The simulated −10 dB return loss bandwidth is 25% for the first frequency band (1.36–1.77 GHz), 24% for the second band (1.96–2.50 GHz), 14% for the third band (3.54–4.09 GHz), and 20% for the last band (5.07–6.25 GHz). These frequency bands cover the commercial frequency bands, such as GPS, WLAN, 4G-LTE, 5G, WiMAX, Bluetooth, and satellite communications (see Table 4).

The surface current amplitude diagram and current vector distribution diagram of the antenna radiator at the centre frequencies of 1.6, 2.35, 3.8, and 5.85 GHz are shown in Figures 9(a)–9(d). For the frequency band with a centre frequency of 1.6 GHz, the left and right slots of the monopole exhibit larger currents (see Figure 9(a)). As the frequency increases, the current is more concentrated on the gaps in the four directions. For the frequency band with a centre frequency of 5.85 GHz, the current reaches a relative maximum value on the four slits of the radiator (see Figure 9(d)).

The 3D gain pattern and E/H-plane radiation pattern of the antenna at the centre frequencies of 1.6, 2.35, 3.8, and 5.85 GHz are shown in Figures 10 and 11. The display gains are 3, 3.74, 5, and 4.99 dBi, respectively. It can be seen that the E-plane and H-plane are omnidirectional in the low-frequency bands of 1.6 and 2.35 GHz, whereas the other two frequency bands are almost omnidirectional. Sidelobes are generated at the centre frequencies of 3.8 and 5.85 GHz, and the degree of cross-polarisation is low.

3. Fabrication and Measurement Results

The proposed antenna was designed on an FR-4 substrate with a thickness of 1.6 mm and loss tangent of 0.02;

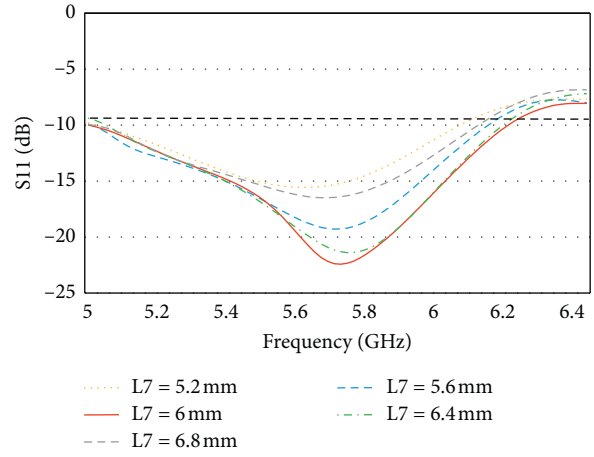

Figure 6: Variation of S11 (dB) for various L_7 lengths.

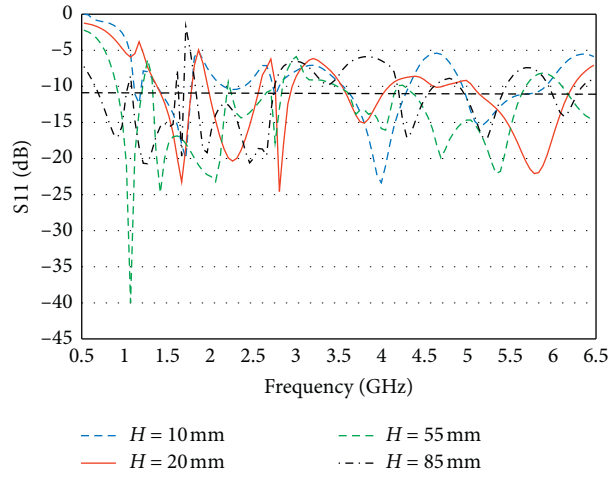

Figure 7: Variation of S11 (dB) for various H lengths.

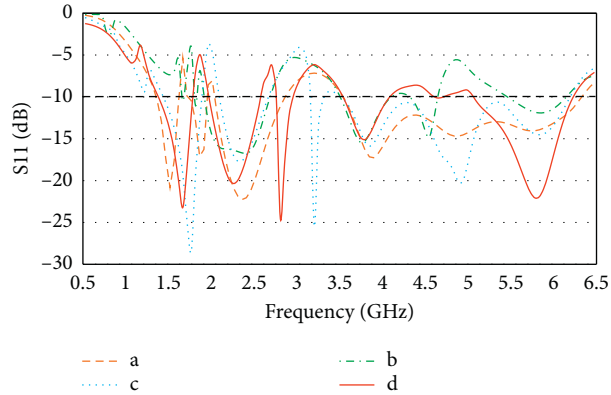

Figure 8: Combined simulated return loss for the antenna evolutions.

furthermore, a 30 μm-thick copper layer was engraved on both sides of the antenna. The front and rear views of the antenna and the experimental test device are shown in Figure 12. The actual performance of the antenna was measured in a microwave electromagnetic anechoic chamber.

The measured and simulated antennas are in the −10 dB return loss frequency band, as shown in Figure 13. The bandwidth of the −10 dB return loss covers roughly the same frequency band as the simulation, as shown in Table 3. The measured and simulated results obtained for

Table 4: Simulated and measured frequency bands covered by the antenna.

Band no.	Bandwidth (measurement)	Bandwidth (simulation)	Covered commercial bands
1	1.58–1.77 GHz (12%)	1.36–1.77 GHz (25%)	GPS (1.575–1.625 GHz), DCS (1.71–1.88 GHz)
2	2.1–2.50 GHz (17%)	1.96–2.50 GHz (24%)	Bluetooth (2.4–2.485 GHz), WLAN (2.4–2.4835 GHz), LTE Band40 (2300–2400 MHz), ISM Band (2.420–2.4835 GHz), iMAX (2.3 GHz), SCDMA (1,880–2,025 MHz and 2,300–2,400 MHz supplementary)
3	3.61–4.09 GHz (12%)	3.54–4.09 GHz (14%)	LTE42/43 (3.4–3.8 GHz), WiMAX (3.3–3.8 GHz)
4	4.75–6.5 GHz (36%)	5.07–6.25 GHz (20%)	WLAN (802.11a/n:5.15–5.35 GHz), 5G (5.725–5.825 GHz)

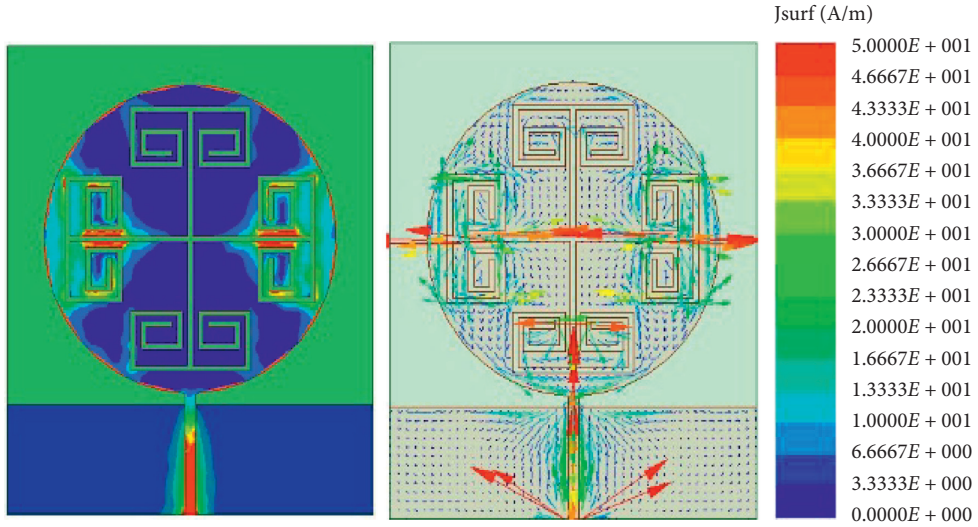

(a)

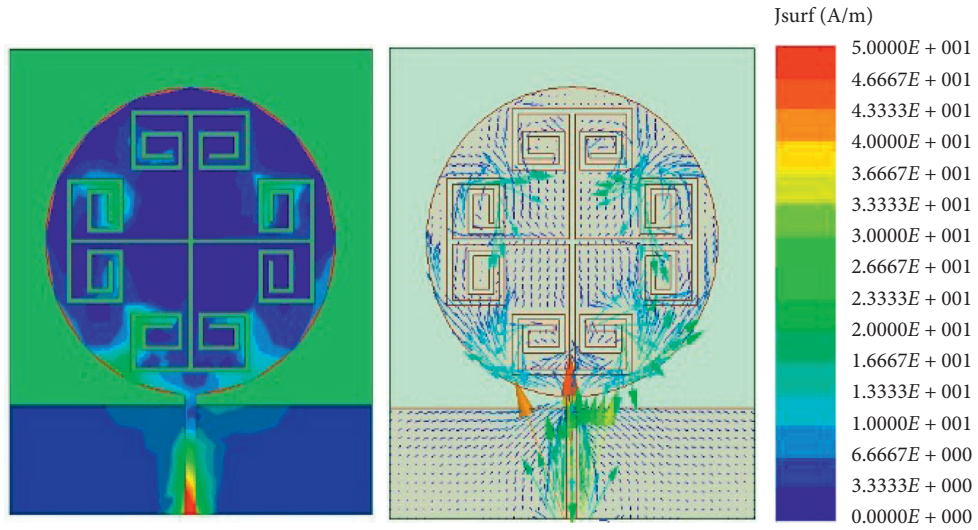

(b)

Figure 9: Continued.

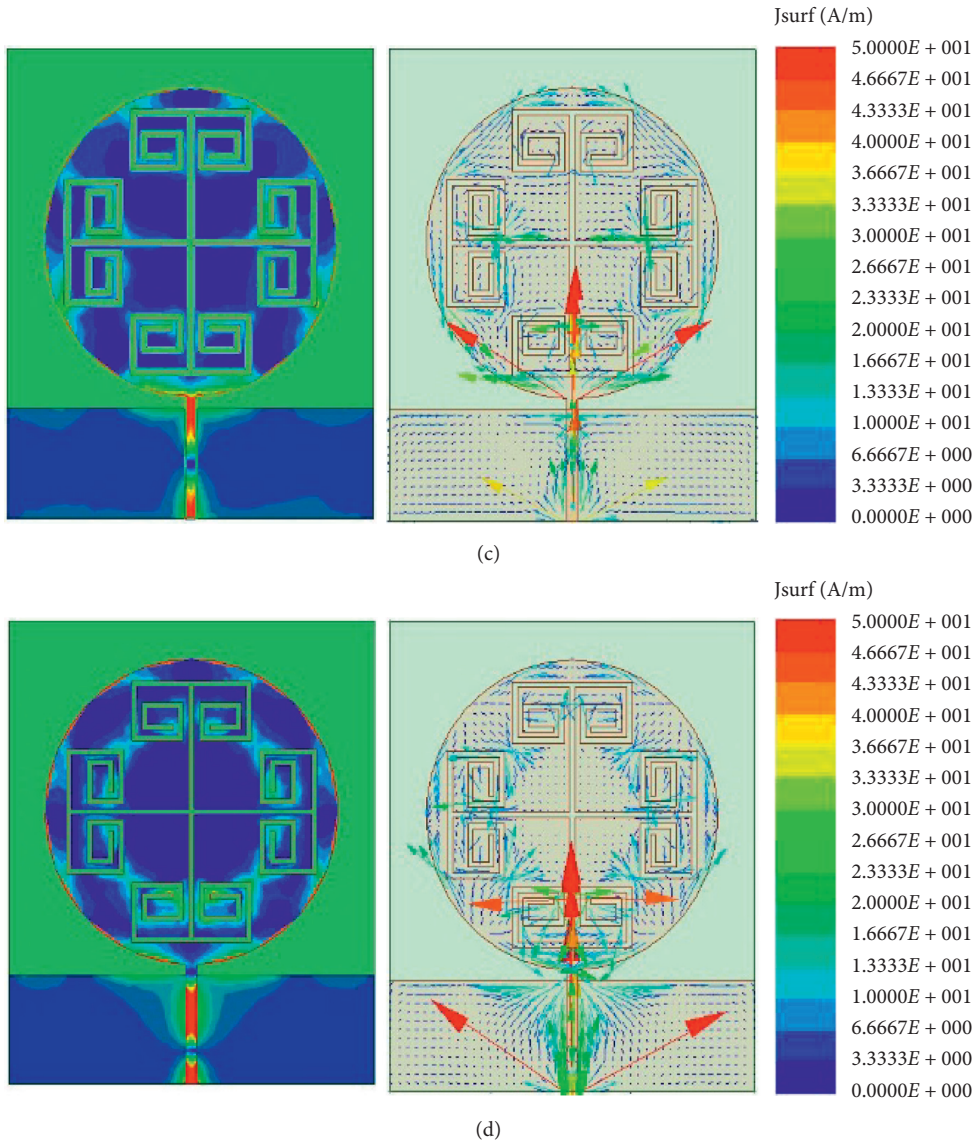

Figure 9: Current amplitude and vector distribution of the antenna at (a) 1.6 GHz, (b) 2.35 GHz, (c) 3.8 GHz, and (d) 5.85 GHz.

the return loss are in good agreement with each other, and the minor differences observed can be attributed to several reasons.

Figures 14(a)–14(d) show the 3D radiation pattern, and Figures 15(a)–15(d) show E/H-plane radiation patterns measured by the antenna at 1.6, 2.35, 3.8, and 5.85 GHz. The measurement result is again in good agreement with the simulation. The manufactured antenna exhibits good radiation characteristics in all frequency bands and is omnidirectional on the H-plane. However, some differences between the experimental and simulated data can also be observed in this case and can be due to several reasons.

As shown in Figure 16, the actual gain and radiation efficiency of the antenna were measured in an anechoic chamber. The background of the available frequency bands in the picture is light blue. The actual gain in the 1.58–1.77 GHz frequency band is 0.5–2 dBi and the radiation efficiency is 45–65%, the actual gain in the 2.1–2.50 GHz frequency band is 2–3.6 dBi and the radiation efficiency is 55–75%, the actual gain in the 3.61–4.09 GHz frequency band is 3.8–4.1 dBi and the radiation efficiency is 62–81%, and the actual gain in the 4.75–6.5 GHz frequency band is 3–5.9 dBi and the radiation efficiency is 58–72%. The actual efficiency of the antenna is between 10% and 70% in the low-frequency range, whereas the actual efficiency in the high-frequency range exceeds 69%. The efficiency and gain meet the requirements within the available range, and the frequency band coverage is not affected in other places. The presence of a stop band at 1.9 GHz leads to an efficiency of 10%, which can better improve the isolation of the antenna frequency band.

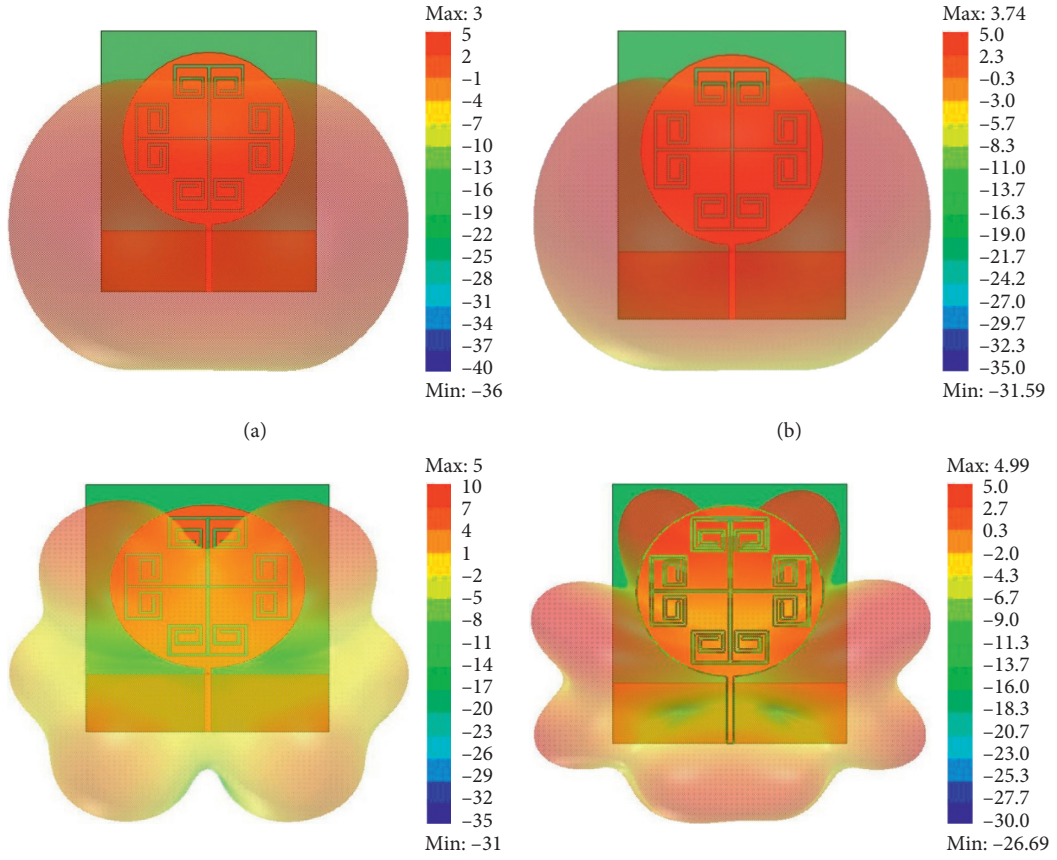

Figure 10: 3D radiation patterns at (a) 1.6 GHz, (b) 2.35 GHz, (c) 3.8 GHz, and (d) 5.85 GHz.

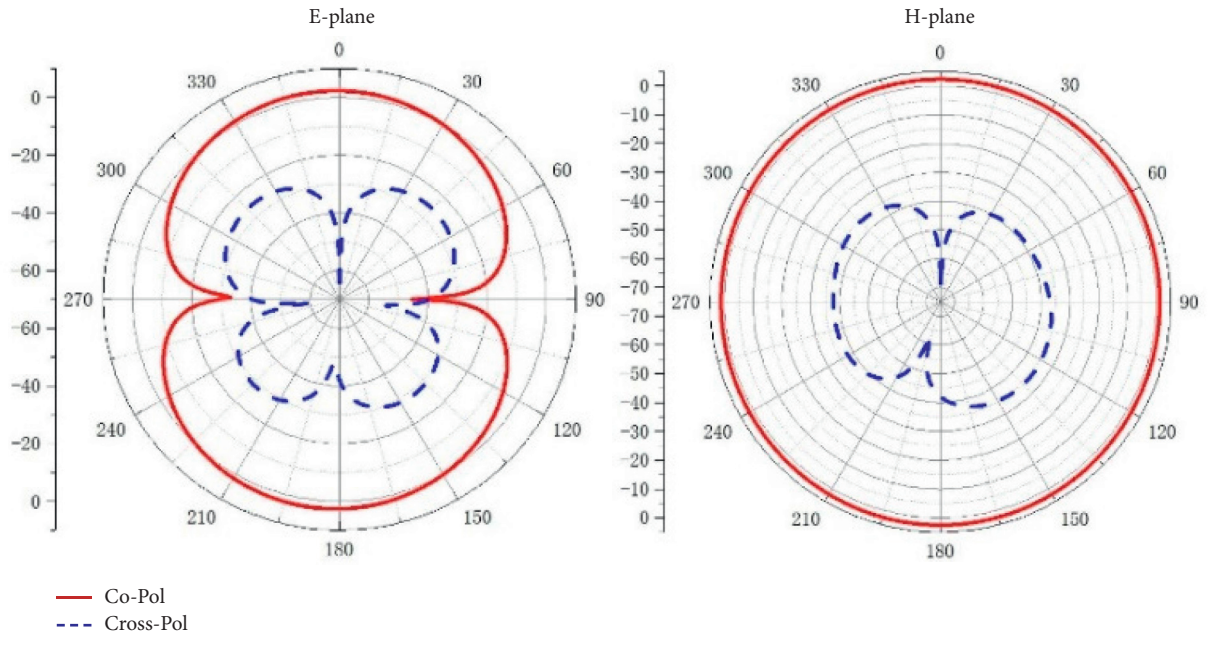

(a)

Figure 11: Continued.

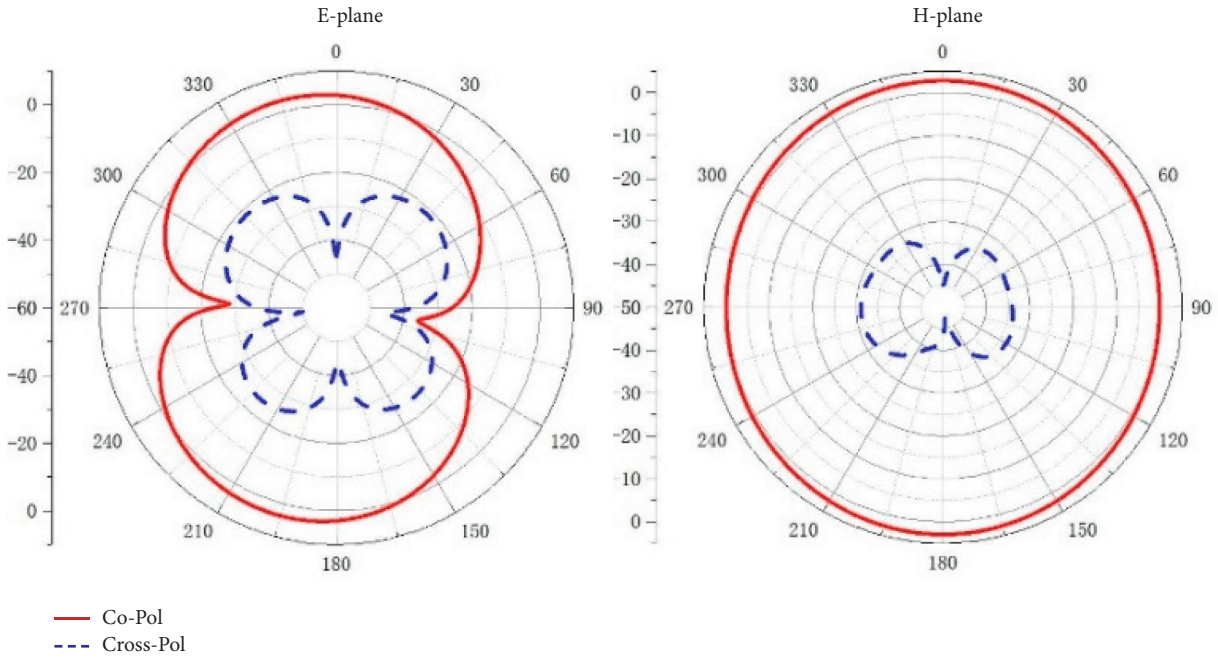

(b)

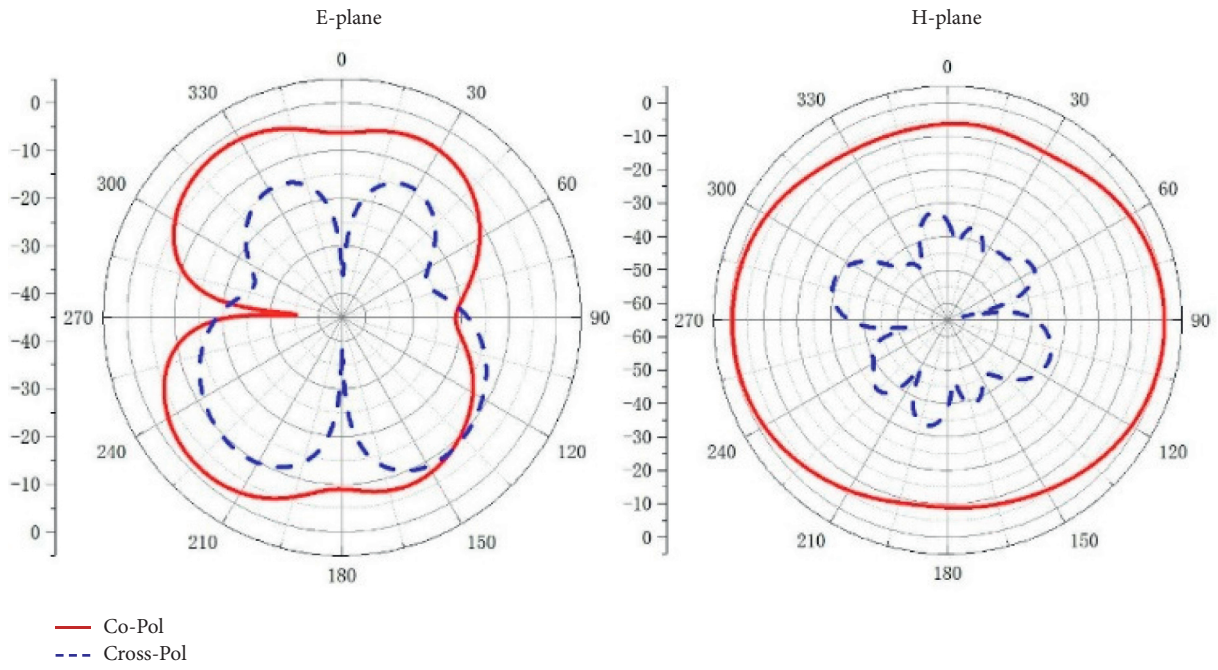

(c)

Figure 11: Continued.

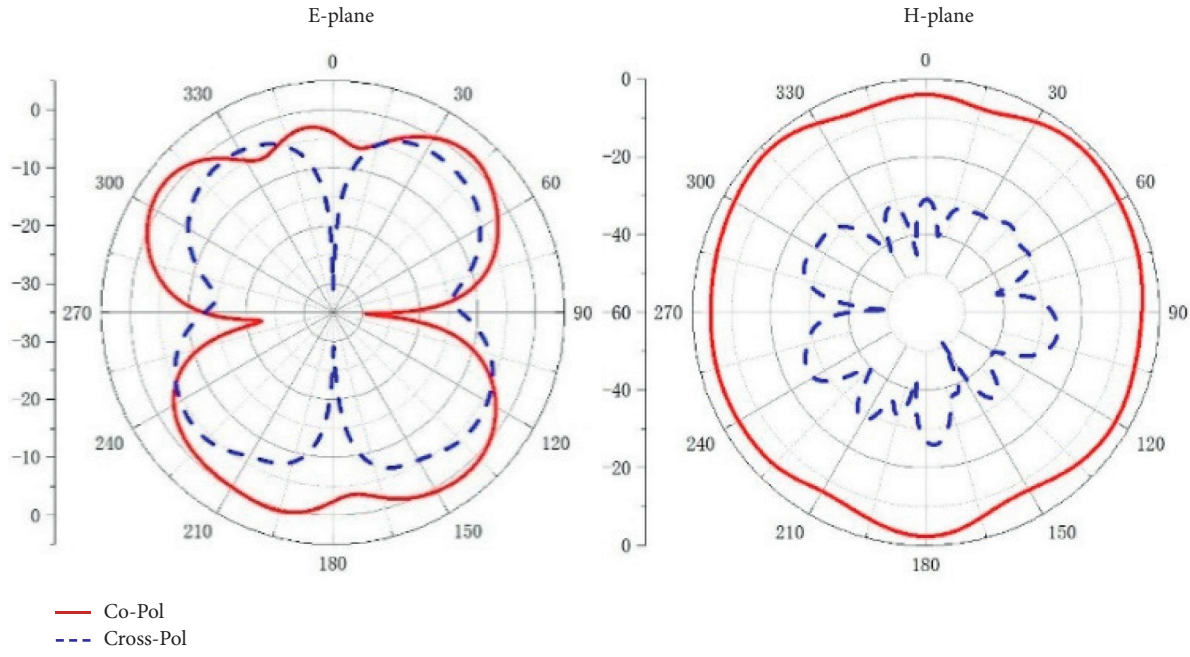

(d)

Figure 11: E- and H-plane radiation patterns at (a) 1.6 GHz, (b) 2.35 GHz, (c) 3.8 GHz, and (d) 5.85 GHz.

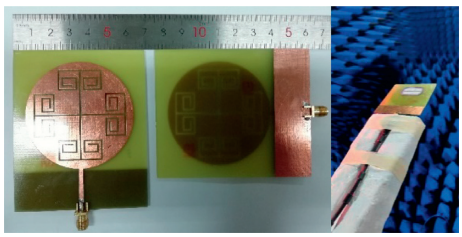

Figure 12: Fabricated antenna prototype and experimental test setup in an anechoic chamber.

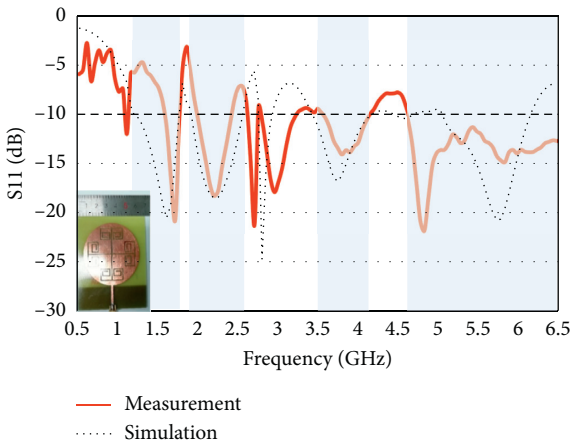

Figure 13: Measurement and simulation of S11 of the antenna.

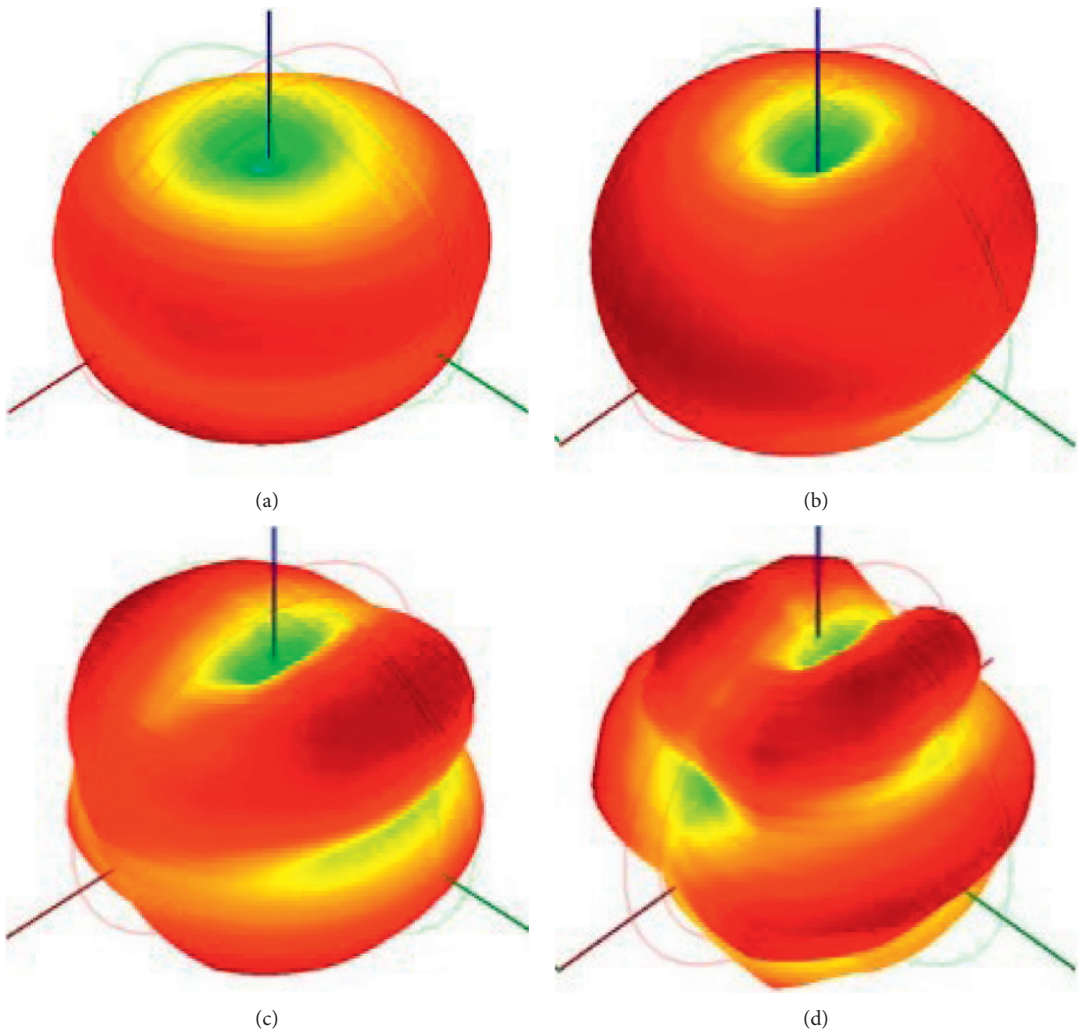

(a) (b) (c) (d)

Figure 14: Antenna measurement 3D radiation pattern at (a) 1.6 GHz, (b) 2.35 GHz, (c) 3.8 GHz, and (d) 5.85 GHz.

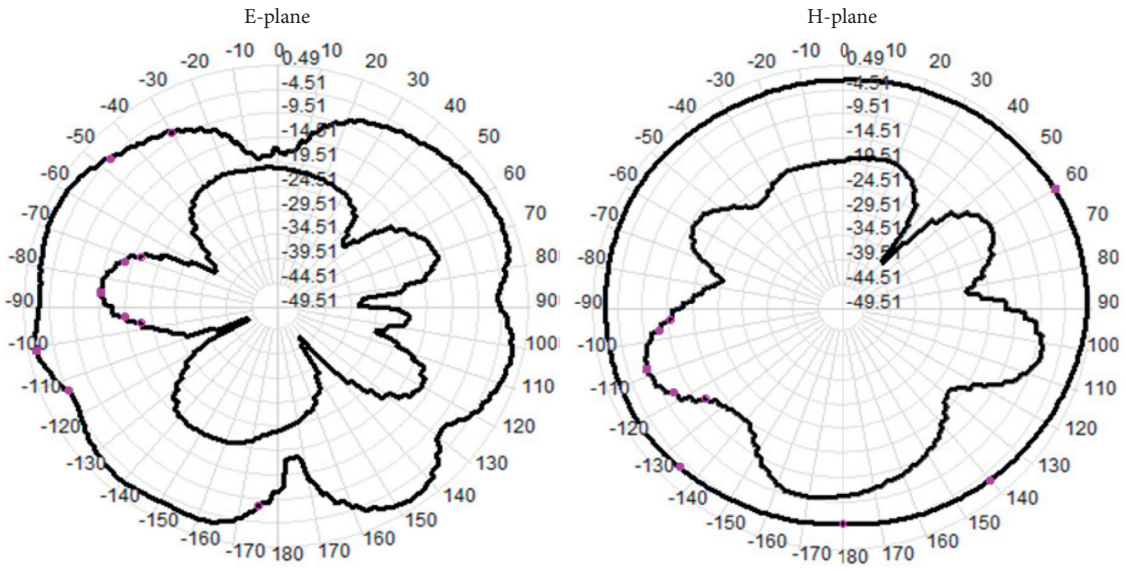

(a)

Figure 15: Continued.

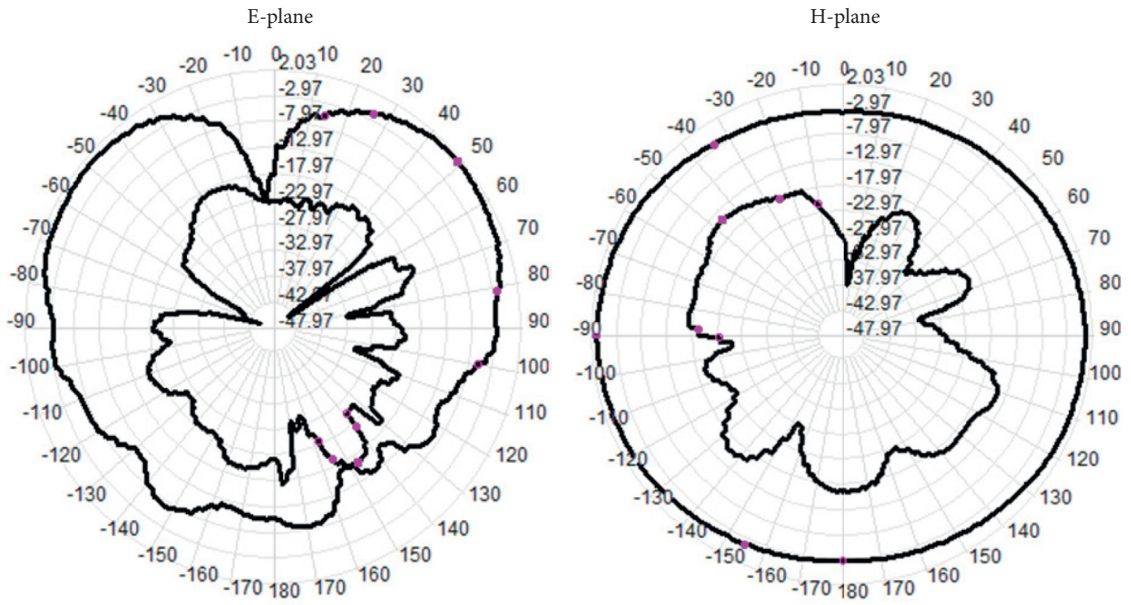

(b)

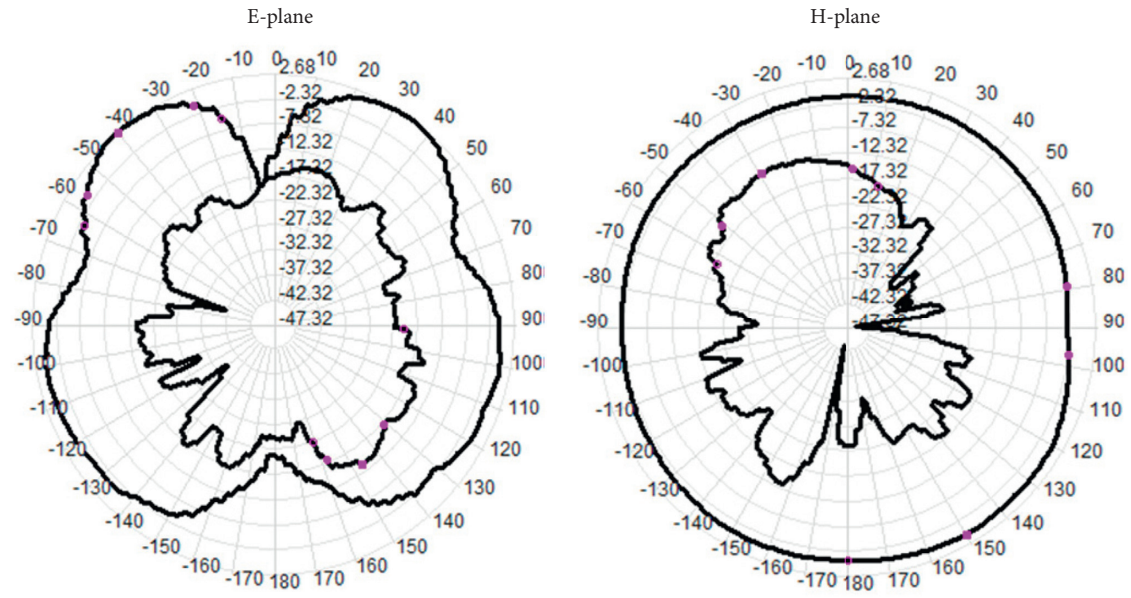

(c)

Figure 15: Continued.

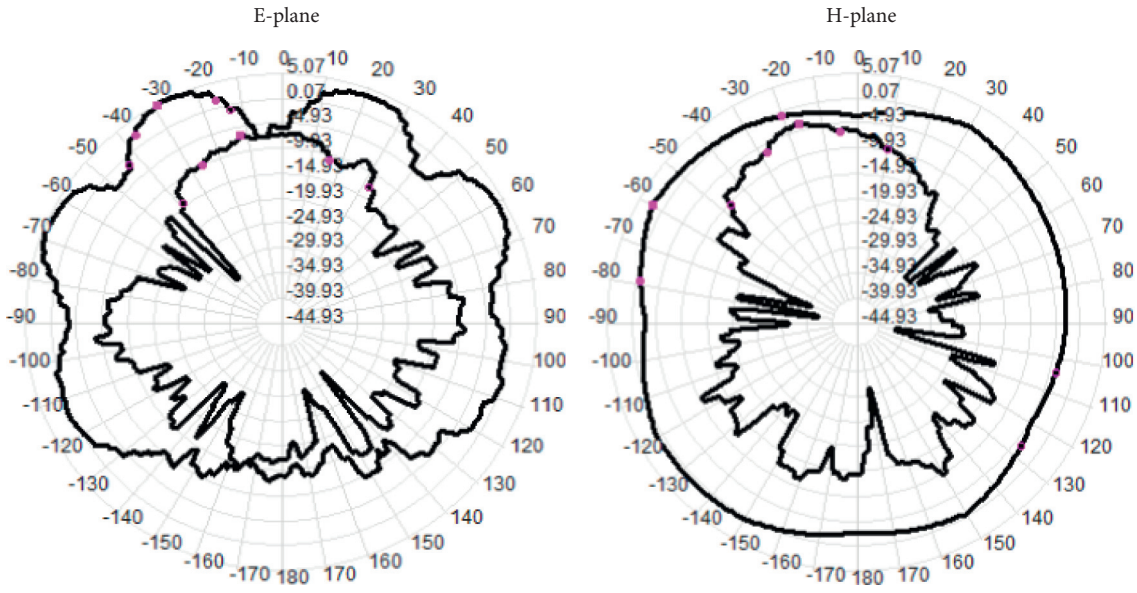

(d)

Figure 15: E/H-plane radiation patterns at (a) 1.6 GHz, (b) 2.35 GHz, (c) 3.8 GHz, and (d) 5.85 GHz.

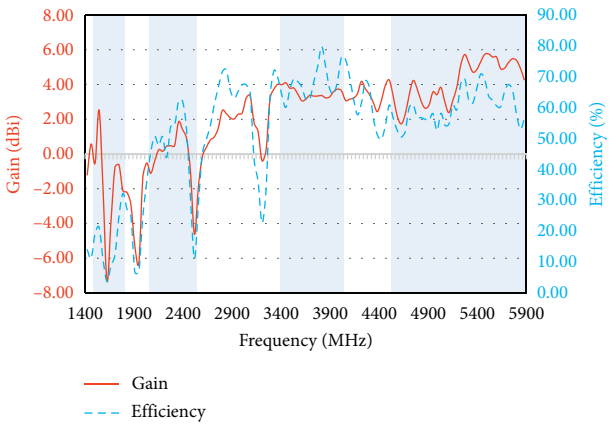

Figure 16: Measured gain and efficiency curves.

4. Conclusions

In this study, a small multiband planar antenna with classical "回" pattern panes was developed for application in the commercial frequency bands, such as GPS, DCS, Bluetooth, WLAN, LTE Band40, WiMAX, SCDMA, 5G, and LTE42/43. The frequency band and bandwidth were found to be 1.58–1.77 GHz (12%), 2.1–2.50 GHz (17%), 3.61–4.09 GHz (12%), and 4.75–6.5 GHz (36%). The radiation direction of the antenna was found to be omnidirectional, and the antenna simulation and performance test confirmed the good performance of the antenna. Overall, it was found that the proposed antenna exhibits good radiation characteristics, is small and light, and is thus suitable for most wireless applications.

Data Availability

The data used to support the findings of this study are included within the article.

Conflicts of Interest

The authors declare that they have no conflicts of interest.

Acknowledgments

This work was supported in part by the National Key R&D Project (no. 2020YFC1511805), National Natural Science Foundation of China (no. 61663014), Hebei Higher Education Teaching Reform Project (Grant no. 2018GJJG477), and Fundamental Research Funds for the Central Universities (Grant nos. 3142018048 and 3142018047).

References

[1] X.Z. Zhu, J.L. Zhang, T. Cui, and Z.Qi Zheng, "A dual-broadband printed dipole antenna for 2G/3G/4G base station applications," *International Journal of Antennas and Propagation*, vol. 2019, Article ID 4345819, 2019.

[2] Z. Yu, J. Yu, X. Ran, and C. Zhu, "A novel ancient coin-like fractal multiband Antenna for wireless applications," *International Journal of Antennas and Propagation*, vol. 2017, Article ID 6459286, 2017.

[3] J. Y. Deng, J. Yao, and L. X. Guo, "Compact multiband antenna for mobile terminal applications," *Microwave and Optical Technology Letters*, vol. 60, no. 7, pp. 1691–1696, 2018.

[4] M. J. Jeong, N. Hussain, H. U. Bong et al., "Ultrawideband microstrip patch antenna with quadruple band notch characteristic using negative permittivity unit cells," *Microwave and Optical Technology Letters*, vol. 62, no. 2, pp. 816–824, 2020.

[5] J. Park, M. Jeong, N. Hussain, S. Rhee, P. Kim, and N. Kim, "Design and fabrication of triple-band folded dipole antenna for GPS/DCS/WLAN/WiMAX applications," *Microwave and Optical Technology Letters*, vol. 61, no. 5, pp. 1328–1332, 2019.

[6] M. Borhani, P. Rezaei, and A. Valizade, "Design of a reconfigurable miniaturized microstrip antenna for

switchable multiband systems," *IEEE Antennas and Wireless Propagation Letters*, vol. 15, 2016.

[7] J. S. Khinda, M. R. Tripathy, and D. Gambhir, "Multi-edged wideband rectangular microstrip fractal antenna array for C- and X-band wireless applications," *Journal of Circuits Systems and Computers*, vol. 26, no. 4, 2017.

[8] W.-C. Weng and C.-L. Hung, "An H-fractal antenna for multiband Applications," *IEEE Antennas and Wireless Propagation Letters*, vol. 13, 2014.

[9] S. Singhal, P. Singh, and A. Kumar Singh, "Asymmetrically CPW-fed octagonal sierpinski UWB fractal antenna," *Microwave and Optical Technology Letters*, vol. 58, no. 7, pp. 1738–1745, 2016.

[10] O. Abu Safia, M. Nedil, L. Talbi, and K. Hettak, "Coplanar waveguide-fed rose-curve shape UWB monopole antenna with dual-notch characteristics," *IET Microwaves, Antennas & Propagation*, vol. 12, no. 7, 2018.

[11] N. T. Thanh, Y. Yang, K. Y. Lee, and K. C. Hwang, "Dual circularlypolarized spidron fractal slot antenna," *Electromagnetics*, vol. 37, no. 1, 2017.

[12] Y. Braham Chaouche, I. Messaoudene, B.4 Ismail, M. Nedil, and F. Bouttout, "Compact coplanar waveguide-fed reconfigurable fractal antenna for switchable multiband systems," *IET Microwaves, Antennas & Propagation*, vol. 13, no. 1, 2018.

[13] X.-X. Yang, G.-N. Tan, B. Han, and H.-G. Xue, "Millimeter wave fabry-perot resonator antenna fed by CPW with high gain and broadband," *International Journal of Antennas and Propagation*, vol. 2016, Article ID 3032684, 2016.

[14] A. K. Gautam, L. Kumar, B. Kumar Kanaujia, and K. Rambabu, "Design of compact F-shaped slot triple-band Antenna for WLAN/WiMAX applications," *IEEE Antennas and Wireless Propagation Letters*, vol. 64, no. 3, 2016.

[15] D. Upadhyay and I. Acharya, "A novel modified star fractal monopole antenna for UWB applications," in *Proceedings of the 2015 Twelfth International Conference on Wireless and Optical Communications Networks*, Bangalore, India, September 2015.

[16] S. Dhar, K. Patra, R. Ghatak, B. Gupta, and D. R. Poddar, "A dielectric resonator-loaded minkowski fractal-shaped slot loop heptaband Antenna," *IEEE Antennas and Wireless Propagation*, vol. 63, no. 4, 2015.

[17] L. Wang, J. Yu, T. Xie, Z. Yu, B. Liang, and X. Xu, "The design of a multi-band bionic antenna for mobile terminals," *International Journal of RF and Microwave Computer-Aided Engineering*, vol. 31, no. 6, 2021.

[18] T. Chen, Y. Chen, and R. Jian, "A wideband differential-fed microstrip patch antenna based on radiation of three resonant modes," *International Journal of Antennas and Propagation*, vol. 2019, Article ID 4656141, , 2019.

[19] R. K. Yadav, J. Kishor, and R. L. Yadava, "A Chaucer microstrip fractal antenna for mobile applications," *Journal of Communications Technology and Electronics*, vol. 61, no. 2, pp. 138–144, 2016.

[20] J. Kulkarni, A. Desai, and C.-Y. Desmond Sim, "Wideband Four-Port MIMO antenna array with high isolation for future wireless systems," *International Journal of Electronics and Communications*, vol. 128, Article ID 153507, 2021.

[21] J. Kulkarni and C.-Y.-D. Sim, "Wideband cpw-fed oval-shaped monopole antenna for wi-fi5 and wi-fi6 applications," *Progress In Electromagnetics Research C*, vol. 107, pp. 173–182, 2021.